
ORIGINAL ARTICLE

Journal Section

Nonparametric Independent Component Analysis for the Sources with Mixed Spectra

Seonjoo Lee, PhD¹ | Haipeng Shen, PhD² | Young K. Truong, PhD³

¹Mental Health Data Science, The Research Foundation in Mental Hygen Inc. and Department of Biostatistics and Psychiatry, Columbia University, U.S.A.

²Innovation and Information Management, Faculty of Business and Economics, University of Hong Kong, Hong Kong, China

³Department of Biostatistics, University of North Carolina at Chapel hill, Chapel hill, North Carolina, U.S.A.

Correspondence

Seonjoo Lee PhD, Mental Health Data Science, The Research Foundation in Mental Hygen Inc. and Department of Biostatistics and Psychiatry, Columbia University, U.S.A
Email: seonjoo.lee@nyspi.columbia.edu

Funding information

Lee's work is partially supported by NIH grant R01AG062578. Shen's work is partially supported by HKSAR CRF grant C7162-20G and HKU BRC grant.

Independent component analysis (ICA) is a blind source separation method to recover source signals of interest from their mixtures. Most existing ICA procedures assume independent sampling. Second-order-statistics-based source separation methods have been developed based on parametric time series models for the mixtures from the auto-correlated sources. However, the second-order-statistics-based methods cannot separate the sources accurately when the sources have temporal autocorrelations with mixed spectra. To address this issue, we propose a new ICA method by estimating spectral density functions and line spectra of the source signals using cubic splines and indicator functions, respectively. The mixed spectra and the mixing matrix are estimated by maximizing the Whittle likelihood function. We illustrate the performance of the proposed method through simulation experiments and an EEG data application. The numerical results indicate that our approach outperforms existing ICA methods, including SOBI algorithms. In addition, we investigate the asymptotic behavior of the proposed method.

KEYWORDS

blind source separation, encephalography, independent

Abbreviations: ICA, independent component analysis

component analysis, log-spline density estimation, spectral density estimation, Whittle likelihood

1 | INTRODUCTION

Independent component analysis (ICA) is a popular blind source separation method. A typical instantaneous ICA expresses a set of observed mixed signals as linear combinations of independent latent sources (or components):

$$\mathbf{X}_{M \times T} = \mathbf{A}_{M \times M} \mathbf{S}_{M \times T}, \quad (1)$$

where \mathbf{X} is an $M \times T$ observed matrix of the M mixed signals, \mathbf{A} is a non-random mixing matrix, and \mathbf{S} is the matrix of *independent* source signals. Under appropriate conditions on \mathbf{A} , the source can be recovered as

$$\mathbf{S} = \mathbf{W}\mathbf{X}, \quad \mathbf{W} = \mathbf{A}^{-1}, \quad (2)$$

by estimating the unmixing matrix \mathbf{W} , which maximizes independence criteria of the estimated sources.

Extensive literature reviews about methodological development and applications for ICA can be found in [1], [2], [3] and [4]. More specifically, it has many important applications in acoustic signal processing [1]; finance [5]; medical image analysis, such as functional magnetic resonance imaging (fMRI) [6], electroencephalography (EEG), and magnetoencephalography (MEG) [7]; and system monitoring [8].

Most early works are based on information theory, including JADE [9], Infomax [10, 11], and fastICA [1]. Later works are based on maximum likelihood using nonparametric density estimation [12, 13, 14, 15, 16, 17, 18]. Recent works attempt to directly measure independence using characteristic functions [19, 20, 21] and distance covariance [22]. When the sources are autocorrelated, second-order-statistics-based methods have been developed. Examples include joint-diagonalization of the covariance matrix and several autocovariance matrices at different lags [23, 24] and Whittle likelihood-based methods [25, 26, 27].

In biomedical applications like EEG, the sources possibly include sinusoidal signals with line spectra (or atoms) in the spectral domain. Although the ARMA model or autocovariance can approximate sharp line spectra, the estimation is often biased due to the Dirichlet kernel effect. To address this gap, we propose a new ICA method by employing the flexible source models and log-spline density estimation procedure to the ICA. [28] proposed a flexible model for the sources with mixed spectra; that is, the sources consist of sinusoidal signals and stochastic signals. The log-spline spectral density estimation procedure estimates the spectral density function, which is determined by the stochastic signal, with B-spline basis functions, and detects line spectra, which are determined by sinusoidal signals, based on Fourier frequencies. We take an iterative estimation procedure to estimate the unmixing matrix \mathbf{W} and the spectral densities of the sources. In spectral density estimation, the numbers and locations of the knots of B-splines and the atoms are determined using Bayesian Information Criteria (BIC). Our simulation studies show better performance over the currently existing ICA algorithms. Finally, we investigated the asymptotic properties of the proposed method.

The rest of the paper is laid out as follows: Section 2 reviews the Whittle likelihood-based ICA for autocorrelated sources and source models with possibly mixed spectra followed by the new ICA algorithm via nonparametric spectral density estimation (cICA-LSP). We show by intensive simulation studies that our newly proposed method performs better than other existing ICA algorithms in Section 3. In simulation studies, we also examine the performance of our new approach using real sound data. In Section 4, we also analyze EEG data. In Section 5, asymptotic properties of

cICA-LSP are presented.

2 | INDEPENDENT COMPONENT ANALYSIS VIA NONPARAMETRIC SPECTRAL DENSITY ESTIMATION

This section proposes a new ICA procedure via maximizing the Whittle likelihood with the nonparametric spectral density estimation. First, we review the Whittle likelihood-based ICA method in Section 2.1, followed by a new source model and nonparametric spectral density estimation in Section 2.2. Finally, Section 2.3 presents the details of the cICA-LSP algorithm.

2.1 | Review of the Whittle likelihood-based ICA

In this section, we review the Whittle likelihood-based ICA method proposed by [26] for temporally autocorrelated sources. For an observed M -dimensional vector process $\mathbf{X}(t) = (X_1(t), \dots, X_M(t))^T$ with zero mean and the covariance function $\gamma_X(u) = \text{Cov}(\mathbf{X}(t), \mathbf{X}(t+u))$ and the $M \times M$ spectral density matrix $\mathbf{F}_X(\cdot)$. The discrete Fourier transform (DFT) of \mathbf{X} is given by

$$\mathbf{d}(r_k, \mathbf{X}) = \sum_{k=0}^{T-1} \mathbf{X}(t) \exp\{-ir_k t\}, \quad r_k = \frac{2\pi k}{T}, \quad k \in \{0, \dots, T-1\},$$

and the second order periodogram by $\tilde{\mathbf{f}}(r_k, \mathbf{X}) = \frac{1}{2\pi T} \mathbf{d}(r_k, \mathbf{X}) \mathbf{d}^*(r_k, \mathbf{X})$, where \mathbf{d}^* is the conjugate transpose of the vector \mathbf{d} . The spectral density matrix \mathbf{F}_S , the DFT and the second order periodogram of the source signals $\mathbf{S}(t) = (S_1(t), \dots, S_M(t))^T$, $t \in \{0, 1, \dots, T-1\}$, are defined similarly. Note that the source spectral density matrix is diagonal $\mathbf{F}_S = \text{diag}(f_1, \dots, f_M)$, where f_j , $j \in \{1, \dots, M\}$ is the spectral density of the j th source because the sources are mutually independent.

By the independence of the sources, the ICA model (2), and the asymptotic properties of the DFT, we derive the Whittle log-likelihood [29]:

$$\mathcal{L}(\mathbf{W}, \mathbf{F}_S; \mathbf{X}) = -\frac{1}{2T} \sum_{j=1}^M \sum_{k=0}^{T-1} \left(\frac{\mathbf{e}_j^T \mathbf{W} \tilde{\mathbf{f}}(r_k, \mathbf{X}) \mathbf{W}^T \mathbf{e}_j}{f_j(r_k)} + \log f_j(r_k) \right) + \log |\det(\mathbf{W})|, \quad (3)$$

where $\mathbf{e}_j = (0, 0, \dots, 1, 0, \dots, 0)^T$ with the j th entry being 1.

Note that [26] parametrized the source spectra using autocorrelation (AR) models, and the unmixing matrix \mathbf{W} was estimated by maximizing (3). The method has shown promising results through simulation studies and was applied to fMRI data to identify brain-functional areas. For biomedical applications, however, some sources may have more complex structures. In EEG experiments, for instance, ICA is often applied to reduce noise artifacts or sometimes to detect neuronal signals. Some potential sources of interest are known to have a specific frequency range, such as the alpha rhythm (a neural oscillation) with a frequency range between 8–12 Hz. In the spectral domain of time series analysis, such a source has a continuous spectral density (for the background noise) mixed with a discrete real biological component called the line spectrum. The AR model is generally flexible to approximate a wide variety of continuous spectral density functions, while some harmonic processes are known to be useful for modeling line spectra. In this paper, we employ a nonparametric spectral density estimation technique to improve the flexibility in

simultaneously estimating the continuous and line spectra of the sources.

2.2 | Source Model

To model source spectral density functions, we consider sources with mixed spectra, studied broadly in literature. In this section, we review a mixed spectral density model proposed by [28].

Consider a univariate second order stationary process $\{S_j(t)\}$ with mean zero and covariance function $\gamma_j(u) = \text{Cov}(S_j(t), S_j(t+u))$ for $j \in \{1, \dots, M\}$. Assume that each source time series has the form

$$S_j(t) = \sum_{p=1}^{P_j} R_{jp} \cos(t\omega_{jp} + \phi_{jp}) + Y_j(t), \quad t \in \{0, \dots, T-1\}, \quad (4)$$

where $0 < \omega_{jp} \leq \pi$; ϕ_{jp} are independent and uniformly distributed on $[-\pi, \pi]$; R_{jp} , $p = 1, \dots, P_j$, are independent, non-negative random variables such that R_{jp}^2 has positive mean $4\rho_{jp}$; and $Y_j(t)$ is a second-order stationary time series with mean zero and spectral density function f_j^c , and is independent of R_{jp} and ϕ_{jp} .

Model (4) satisfies the weak stationary conditions and is very flexible, allowing varying phases and intensities of deterministic terms. In addition, we note that (4) is a very practical model for many applications, such as fMRI or EEG data analysis, because most brain-function-related or physiological signals have mixed spectral densities. Then, the spectral density distribution of the time series $S_j(t)$ is given by

$$F_j(r) = \int_{-\pi}^r f_j^c(u) du + \sum_{u \leq r} f_j^d(u), \quad -\pi \leq r \leq \pi, \quad (5)$$

where its line spectrum is given by

$$f_j^d(r) = \begin{cases} \rho_{jp} & \text{if } r = \pm\lambda_{jp} \\ 0 & \text{otherwise.} \end{cases} \quad (6)$$

Note that f_j^c and f_j^d are symmetric about zero and periodic with period 2π .

The periodogram of each source is given by

$$\bar{f}(r, S_j) = \frac{1}{2\pi T} \left| \sum_{t=0}^{T-1} e^{-irt} S_j(t) \right|^2, \quad -\pi \leq r \leq \pi.$$

Denote the mean spectral density function of each source as $f_j = f_j^c + \frac{T}{2\pi} f_j^d$. The periodogram, $\bar{f}(\frac{2\pi k}{T}, S_j)$, asymptotically follows $f_j(\frac{2\pi k}{T}) E_j$, where $E_j \sim \text{Exp}(1)$ if $k < T/2$ and $E_j \sim \chi_1^2$ if T is even and $k = T/2$, and are asymptotically independent [30].

Below, we describe how to model the mean spectral density functions using a nonparametric scheme. There have been many nonparametric spectral density estimation methods. Examples include smoothing the periodogram [30], minimizing least-square using smoothing splines with cross-validation [31], maximizing the Whittle likelihood via sieve estimation [32], bootstrapping [33], penalized Whittle likelihood [34], log-spline with knot selection based on BIC [28], and local smoothing with adaptive bandwidth selection [35]. Among all, we employ the log-spline spectral density estimation procedure proposed by [28] due to the ability to detect deterministic periodic signals and the convenience

of combining the ICA algorithm.

For each $j \in \{1, \dots, M\}$, write the logarithm of the mean spectral density function as $\varphi_j = \log f_j$. We use a combination of B-splines and dirac delta functions to model the spectral density functions f_j^c and the line spectra f_j^d , respectively.

First, we model the spectral density functions f_j^c . Given the positive integer K_j^c and the sequence $t_{j1}, \dots, t_{jK_j^c}$, with $0 \leq t_{j1} < \dots < t_{jK_j^c} \leq \pi$, let $S_T^{j,c}$ denote the space of cubic polynomial splines s on the interval $[0, t_{j1}], \dots, [t_{jK_j^c}, \pi]$ with the first derivative of s being zero at 0 and π , the third derivative of s being zero at 0 unless $t_{j1} = 0$, and the third derivative of s being zero unless $t_{jK_j^c} = \pi$. Let $B_{jk}, 1 \leq k \leq K_j^c$, denote the usual basis of $S_T^{j,c}$ consisting of B-splines for spline g_j^c . Since the spectral density function f_j^c is symmetric about zero, and is periodic with the period 2π , we have that $f_j^{c'}(0) = f_j^{c'''}(0) = f_j^{c'}(\pi) = f_j^{c'''}(\pi) = 0$ and $\varphi_j^{c'}(0) = \varphi_j^{c'''}(0) = \varphi_j^{c'}(\pi) = \varphi_j^{c'''}(\pi) = 0$. Here, splines g_j^c on $[0, \pi]$ such that $g_j^{c'}(0) = g_j^{c'''}(0) = g_j^{c'}(\pi) = g_j^{c'''}(\pi) = 0$ are considered to model the logarithm of the spectral density function φ_j .

To model line spectrum, we consider the space of dirac delta functions. Given the positive integer K_j^d and the increasing sequence $a_1, \dots, a_{K_j^d} \in \left\{ \frac{2\pi j}{T} : 1 \leq j \leq \frac{T}{2} \right\}$, let $S_T^{j,d}$ be the K_j^d -dimensional space of nonnegative function s on $[0, \pi]$ such that $s = 0$ except $a_1, \dots, a_{K_j^d}$. Set $B_{jk+K_j^c}(\omega) = \delta_{a_j}(\omega), 1 \leq k \leq K_j^d$. Then $B_{1+K_j^c}, \dots, B_{K_j^d+K_j^c}$ is a B-spline basis of $S_T^{j,d}$.

Finally, we combine two procedures described above together to estimate the spectral density. Let S_T^j be the space spanned by B_{j1}, \dots, B_{jK_j} , where $K_j = K_j^c + K_j^d$. Set

$$\begin{aligned} g_j^c &= \beta_{j1} B_{j1} + \dots + \beta_{jK_j^c} B_{jK_j^c}, \\ g_j^d &= \beta_{jK_j^c+1} B_{jK_j^c+1} + \dots + \beta_{jK_j} B_{jK_j}, \end{aligned}$$

with $\beta_{jK_j^c+1}, \dots, \beta_{jK_j} \geq 0$, and

$$g_j(\cdot; \beta) = g_j^c(\cdot; \beta_c) + g_j^d(\cdot; \beta_d) = \beta_{j1} B_{j1}(\cdot) + \dots + \beta_{jK_j} B_{jK_j}(\cdot) = \beta_j^T \mathbf{B}_j(\cdot),$$

with $\beta_j = (\beta_{j1}, \dots, \beta_{jK_j})^T, j = 1, \dots, M$, and $\sum_{j=1}^M K_j = K$ so as to $\beta = (\beta_1^T, \dots, \beta_M^T)^T$ constrained to lie in the subspace Ω of \mathbb{R}^K given by

$$\Omega = \left\{ \beta = (\beta_1^T, \dots, \beta_M^T)^T = (\beta_{j1}, \dots, \beta_{MK_M})^T \in \mathbb{R}^K : \right.$$

$$\text{for each } j, g_j'(0) = g_j'''(0) = g_j'(\pi) = g_j'''(\pi) = 0,$$

$$\left. \text{where } g_j = \beta_{j1} B_{j1}(\cdot) + \dots + \beta_{jK_j} B_{jK_j}(\cdot) \right\}.$$

The Whittle loglikelihood is rewritten in terms of the unknown parameters (\mathbf{W}, β) as

$$\begin{aligned} \mathcal{L}_T(\mathbf{W}, \beta; \mathbf{X}) &= -\frac{1}{2T} \sum_{j=1}^M \sum_{k=0}^{T-1} \left(\frac{\mathbf{e}_j^T \mathbf{W} \bar{\mathbf{f}}(r_k, \mathbf{X}) \mathbf{W}^T \mathbf{e}_j}{\exp\{g_j(r_k; \beta_j)\}} + g_j(r_k; \beta_j) \right) + \log |\det \mathbf{W}| \\ &= -\frac{1}{2T} \sum_{j=1}^M \sum_{k=0}^{T-1} \left(\frac{\mathbf{e}_j^T \mathbf{W} \bar{\mathbf{f}}(r_k, \mathbf{X}) \mathbf{W}^T \mathbf{e}_j}{\exp\{\beta_j^T \mathbf{B}_j(r_k)\}} + \beta_j^T \mathbf{B}_j(r_k) \right) + \log |\det \mathbf{W}|. \end{aligned} \quad (7)$$

Note that when the data are spatially whitened (or sphered), we have $\log |\det \mathbf{W}| = 0$ by the orthonormal condition. Once the Whittle log-likelihood is formulated as above, we can obtain the estimates for the unmixing matrix \mathbf{W} and the estimates of the power spectra by maximizing (3).

Remarks. 1. As a reminder, the approach of [25] assumed that f_j is known, and [26] used the ARMA model to estimate spectral densities. In this paper, we estimate spectral densities using an adaptive nonparametric method that requires weaker assumptions than previous methods and is flexible for mixed spectra.

2. In spectral density estimation, if we fix knots, spectral density estimation becomes a fully parametric approach. In our procedure, we select the number of knots. For detail on the knot selection procedure, see [28].

2.3 | Algorithm

Many ICA algorithms apply (spatial) pre-whitening as a preprocessing step due to many advantages of optimization on the Stiefel manifold [36, 37, 38, 39, 40]. Let $\Sigma_{\mathbf{X}} = \text{Cov} \mathbf{X}$ and $\tilde{\mathbf{X}} = \Sigma_{\mathbf{X}}^{-1/2} \mathbf{X}$. Then, $\text{Cov} \tilde{\mathbf{X}} = \mathbf{I}_{M \times M}$ and (2) is equivalent to $\mathbf{S} = \mathbf{W} \Sigma_{\mathbf{X}}^{1/2} \tilde{\mathbf{X}}$. If we assume $\text{Cov} \mathbf{S} = \mathbf{I}_{M \times M}$, we have $\mathbf{O} = \mathbf{W} \Sigma_{\mathbf{X}}^{1/2}$, be an orthonormal matrix. Now the problem is to solve $\tilde{\mathbf{X}} = \mathbf{O} \mathbf{S}$, restricting the matrix \mathbf{O} on the orthonormal matrices. The covariance matrix $\Sigma_{\mathbf{X}}$ can be estimated by the sample covariance matrix of \mathbf{S} , $\tilde{\Sigma}_{\mathbf{X}} = \frac{1}{T} \sum_{t=0}^{T-1} (\mathbf{X}(t) - \bar{\mathbf{X}}) (\mathbf{X}(t) - \bar{\mathbf{X}})^{\top}$, where $\bar{\mathbf{X}} = \frac{1}{T} \sum_{t=0}^{T-1} \mathbf{X}(t)$. The prewhitened ICA algorithms first estimates an orthogonal unmixing matrix, $\tilde{\mathbf{O}}$, by solving (7), and then estimate the unmixing matrix by $\hat{\mathbf{W}} = \tilde{\mathbf{O}} \tilde{\Sigma}_{\mathbf{X}}^{-1/2}$.

To incorporate the orthonormal constraints, we propose to use Lagrange multiplier. More specifically, we consider minimizing the following penalized negative Whittle log-likelihood,

$$F(\mathbf{O}, \lambda, \beta) = -\mathcal{L}_T(\mathbf{O}, \beta; \tilde{\mathbf{Y}}) + \lambda^{\top} \mathbf{C}, \quad (8)$$

where $\lambda = (\lambda_1, \dots, \lambda_{M(M+1)/2})^{\top}$ is the Lagrange parameter vector, and \mathbf{C} is a $M(M+1)/2$ -dimensional vector with the element being $C_{(j-1)M+k} = (\mathbf{O} \mathbf{O}^{\top} - \mathbf{I}_M)_{jk}$, $j = 1, \dots, M$, $k = 1, \dots, j$. Note that we need only $M(M+1)/2$ constraint functions since $\mathbf{O} \mathbf{O}^{\top} - \mathbf{I}_M$ is symmetric.

In practice, the locations and the number of knots of the spectral densities are not given, so the knot selection procedure is necessary. However, minimizing (8) with the knot selection procedure and the parameters at the same time is computationally expensive. Henceforth, we iteratively estimate the unmixing matrix and the spectral density parameters. In each iteration, given $\tilde{\mathbf{O}}$, we estimate β_j maximizing the Whittle log-likelihood (7). We then select the "optimal" knots using model selection criterion such as Bayesian information criterion (BIC) [41] as described in Section 2.2.

Next, given the estimate $\tilde{\beta}$, we obtain the updated estimate of unmixing matrix \mathbf{O} by minimizing the penalized criteria (8). Since (8) is nonlinear, we used Newton-Raphson method with Lagrange multiplier. To begin with, we find the first and second derivatives of (8) with respect to \mathbf{O} and λ and denote them as

$$\nabla F(\mathbf{O}, \lambda; \beta) = \begin{pmatrix} \nabla_{\mathbf{O}} F \\ \nabla_{\lambda} F \end{pmatrix} = \begin{pmatrix} \frac{\partial F}{\partial \text{vec} \mathbf{O}} \\ \frac{\partial F}{\partial \lambda} \end{pmatrix}$$

and

$$\nabla^2 F(\mathbf{O}, \lambda; \beta) = \begin{pmatrix} \mathbf{H}_1 & \mathbf{H}_2 \\ \mathbf{H}_2^{\top} & 0 \end{pmatrix},$$

where

$$[\mathbf{H}_1]_{jk} = \frac{\partial^2 F}{\partial \text{vec} \mathbf{O}_j \partial \text{vec} \mathbf{O}_k}, \quad [\mathbf{H}_2]_{jk} = \frac{\partial^2 F}{\partial \text{vec} \mathbf{O}_j \partial \lambda_k}.$$

Then we obtain the one-step Newton-Raphson update for \mathbf{W} and λ as

$$\begin{aligned} \mathbf{O}^{(new)} &= \mathbf{O}^{(old)} - \mathbf{H}_1^{-1} \left(\mathbf{I} - \mathbf{H}_2 \left(\mathbf{H}_2^\top \mathbf{H}_1^{-1} \mathbf{H}_2 \right)^{-1} \mathbf{H}_2^\top \mathbf{H}_1^{-1} \right) \nabla_{\mathbf{O}} F \\ &\quad - \mathbf{H}_1^{-1} \mathbf{H}_2 \left(\mathbf{H}_2^\top \mathbf{H}_1^{-1} \mathbf{H}_2 \right)^{-1} \nabla_{\lambda} F, \\ \lambda^{(new)} &= \lambda^{(old)} - \left(\mathbf{H}_2^\top \mathbf{H}_1^{-1} \mathbf{H}_2 \right)^{-1} \mathbf{H}_2^\top \mathbf{H}_1^{-1} \nabla_{\mathbf{O}} F + \left(\mathbf{H}_2^\top \mathbf{H}_1^{-1} \mathbf{H}_2 \right)^{-1} \nabla_{\lambda} F, \end{aligned} \quad (9)$$

where \mathbf{H}_1 , \mathbf{H}_2 , $\nabla_{\mathbf{O}} F$, and $\nabla_{\lambda} F$ depend on $\mathbf{O}^{(old)}$ and $\lambda^{(old)}$.

The procedure to update (\mathbf{W}, λ) and (ϕ, σ^2) will be alternated until convergence. Since ICA methods have permutation and scale ambiguity problem, we use Amari's Distance [42] as the convergence criterion defined as

$$d_{Amari}(\mathbf{M}_1, \mathbf{M}_2) = \frac{1}{M} \sum_{i=1}^M \left(\frac{\sum_{j=1}^M |a_{ij}|}{\max_j |a_{ij}|} - 1 \right) + \frac{1}{M} \sum_{j=1}^M \left(\frac{\sum_{i=1}^M |a_{ij}|}{\max_i |a_{ij}|} - 1 \right), \quad (10)$$

where \mathbf{M}_1 and \mathbf{M}_2 are $M \times M$ matrices, \mathbf{M}_2 is invertible and a_{ij} is the ij th element of $\mathbf{M}_1 \mathbf{M}_2^{-1}$. When the Amari's distance is less than some threshold, the iteration stops. We name this method as cICA-LSP. The algorithm is summarized as follows:

The cICA-LSP Algorithm

Pre-whitening $\tilde{\mathbf{X}} = \hat{\Sigma}_{\mathbf{X}}^{-1/2} \mathbf{X}$.

Initialize $\mathbf{O}^{(old)}, \lambda^{(old)}$.

While the convergence criterion is unsatisfied,

1. For given $\mathbf{O}^{(old)}$, estimate the sources: $\tilde{\mathbf{S}} = \mathbf{O}^{(old)} \tilde{\mathbf{X}}$. For each $j = 1, \dots, M$,
 - a. Select the location and the number of knots and their locations.
 - b. Estimate $\tilde{\beta}_j$.
2. For given $\tilde{\beta}$, update $\mathbf{O}^{(old)}$ and $\lambda^{(old)}$ as

$$\begin{aligned} \mathbf{O}^{(new)} &= \mathbf{O}^{(old)} - \mathbf{H}_1^{-1} \left(\mathbf{I} - \mathbf{H}_2 \left(\mathbf{H}_2^\top \mathbf{H}_1^{-1} \mathbf{H}_2 \right)^{-1} \mathbf{H}_2^\top \mathbf{H}_1^{-1} \right) \nabla_{\mathbf{O}} F \\ &\quad - \mathbf{H}_1^{-1} \mathbf{H}_2 \left(\mathbf{H}_2^\top \mathbf{H}_1^{-1} \mathbf{H}_2 \right)^{-1} \nabla_{\lambda} F, \\ \lambda^{(new)} &= \lambda^{(old)} - \left(\mathbf{H}_2^\top \mathbf{H}_1^{-1} \mathbf{H}_2 \right)^{-1} \mathbf{H}_2^\top \mathbf{H}_1^{-1} \nabla_{\mathbf{O}} F + \left(\mathbf{H}_2^\top \mathbf{H}_1^{-1} \mathbf{H}_2 \right)^{-1} \nabla_{\lambda} F, \end{aligned}$$

where \mathbf{H}_1 , \mathbf{H}_2 , $\nabla_{\mathbf{O}} F$, and $\nabla_{\lambda} F$ depend on $\mathbf{O}^{(old)}$ and $\lambda^{(old)}$.

3. $\mathbf{O}^{(old)} \leftarrow \mathbf{O}^{(new)}, \lambda^{(old)} \leftarrow \lambda^{(new)}$

end

$$\text{Final } \widehat{\mathbf{W}} = \mathbf{O} \widehat{\Sigma}_X^{-1/2}.$$

3 | SIMULATION STUDIES

The first experiment in Section 3.1 is designed to illustrate the performance of the newly proposed algorithm (cICA-LSP). In Section 3.2, we apply the proposed method to real audio signals obtained from three music sources and two randomly generated noise signals.

3.1 | Simulation study I: sources with mixed spectra-Fourier frequency atoms

According to the ICA model (1), we first generate the source matrix \mathbf{S} , consisting of the four ($M = 4$) stationary time series with two different sample sizes ($T = 512, 4096$). The four sources are generated from:

1. $S_1(t) = 2 \sum_{j=1}^3 \cos(\omega_{1j}t + \phi_{1j}) + Y_1(t)$, $Y_1 \sim N(0, 1)$;
2. $S_2(t) = 2 \sum_{j=1}^3 \cos(\omega_{2j}t + \phi_{2j}) + Y_2(t)$, $Y_2 \sim U(-\sqrt{3}, \sqrt{3})$;
3. $S_3(t) = 2 \sum_{j=1}^3 \cos(\omega_{3j}t + \phi_{3j}) + Y_3(t)$, Y_3 : AR(1) with $t(3)/\sqrt{3}$;
4. $S_4(t) = 2 \sum_{j=1}^3 \cos(\omega_{4j}t + \phi_{4j}) + Y_4(t)$, Y_4 : MA(1) with $N(0, 1)$,

where ω_{jk} , $j = 1, 2, 3, 4$, $k = 1, 2, 3$, are chosen as follows: $\omega_1 = \frac{2\pi}{128} (1, 2, 3)^\top$; $\omega_2 = \frac{2\pi}{512} + \frac{2\pi}{64} (1, 2, 3)^\top$; $\omega_3 = \frac{2\pi}{64} (1, 2, 3)^\top$; $\omega_4 = \frac{2\pi}{128} + \frac{2\pi}{64} (1, 2, 3)^\top$.

A 4×4 full-rank mixing matrix \mathbf{W} was randomly generated as

$$\mathbf{W} = \begin{pmatrix} 0.56 & 0.58 & -0.07 & 0.59 \\ -0.41 & 0.84 & 0.10 & 0.34 \\ -0.15 & 0.05 & 0.75 & -0.65 \\ 0.53 & -0.83 & -0.08 & 0.13 \end{pmatrix}.$$

We also performed the simulation experiments for multiple randomly generated \mathbf{W} s to evaluate the uniform performance across the true unmixing matrix (Supplementary). The data matrix \mathbf{X} is then obtained by multiplying \mathbf{A} and \mathbf{S} : $\mathbf{X} = \mathbf{A}\mathbf{S}$. The simulation is replicated 100 times. The performance of cICA-LSP is compared to the existing popular methods, JADE [9], fastICA [1], JADE-SOBI [23], SOBIN, SOBIdefl [24], and cICA-YW [26].

The Amari distance [42] described in Section 2.3 is used as a performance comparison criterion between various ICA algorithms. Figure 1 shows the boxplots of the Amari error for each method with different sample sizes. Since JADE and fastICA performed far worse than the methods that handle autocorrelations, we did not include those two methods here. The full simulation results are reported in the appendix (Figure 7). The cICA-LSP performed better than the existing methods across the different sample sizes.

3.2 | Audio Sound Example

In this section, we apply the proposed method to a mixture of three music sounds and two simulated noise artifacts. Each music signal is extracted a length 4 seconds and sampled 11025Hz resulting 44100 time points. Two noise signals

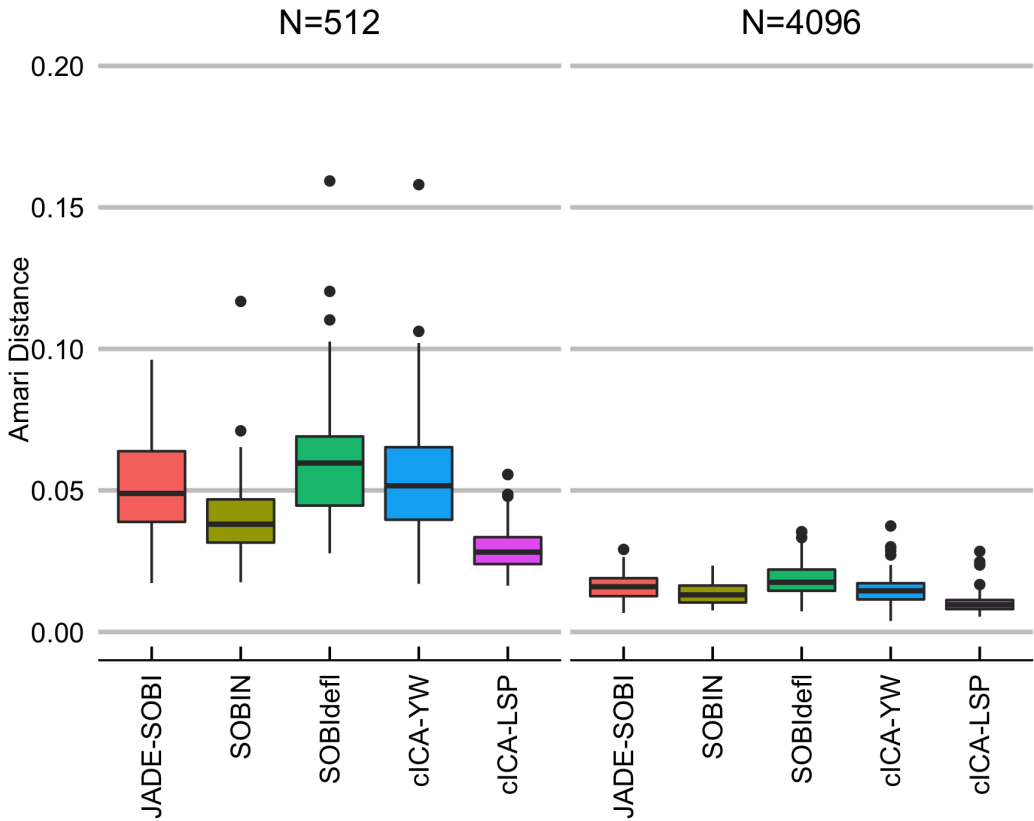


FIGURE 1 Simulation Study I: Performance comparisons for sources with mixed spectra of atoms at Fourier frequency. One hundred simulation runs are performed with different sample sizes (512, 4096). In each simulation run, 4 sources with mixed spectra are generated and are mixed through a 4×4 mixing matrix. The boxplots show the Amari distance between the true unmixing matrix and the estimated unmixing matrix obtained by various ICA methods. The cICA-LSP provides more accurate estimates than the other existing methods.

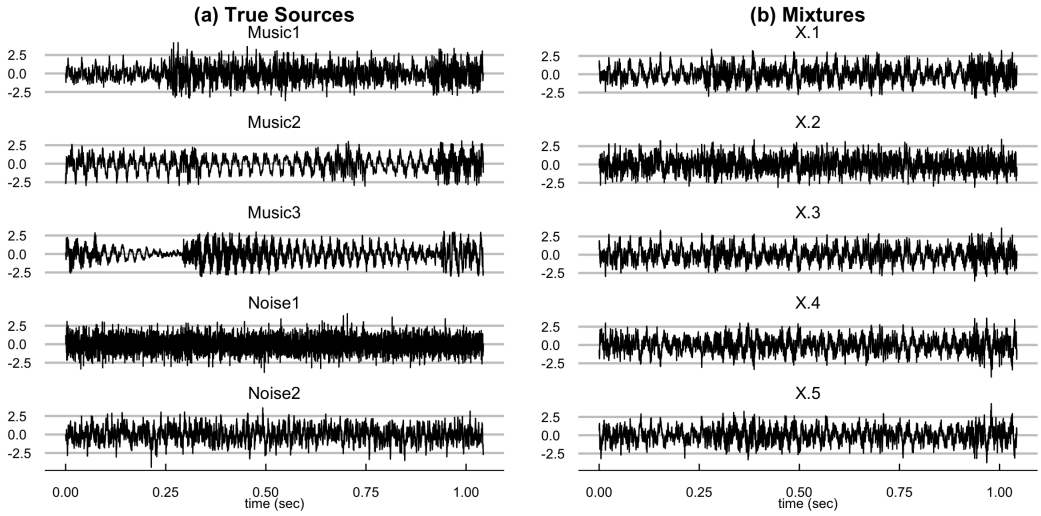


FIGURE 2 The source and mixed signals. Three music sounds and two simulated noise artifacts are mixed with a randomly generated matrix.

are generated as:

- $N_1(t) = 2 \sin(0.036\pi t + 0.1234) + z_1(t)$, $z_1 \sim N(0, 1)$;
- $N_2(t) = 2 \cos(0.007\pi t) + z_2(t)$, $z_2(t) \sim AR(0.8)$.

To generate noisier signals, we generated noise from the logistic distribution for N_2 [43]. The five signals are mixed with a randomly generated 5-by-5 matrix, and the mixed signals are separated using the cICA-LSP algorithm and compared with other ICA algorithms. Figure 2 displays the true sources (S) and the mixture (X) in panels (a) and (b), respectively.

To compare the performance of the ICA algorithms, we consider two criteria: correlations between the estimated sources and the true sources; Amari error between the true unmixing matrix and estimated matrices. Figure 3 shows the correlation matrices obtained by seven ICA methods. Due to the sign and permutation ambiguity of ICA algorithms, we report absolute values of correlations and reordered the row of the matrix according to the highest correlation with the true sources. Each panel represents a five-by-five correlation matrix, and each entry is colored with a gray color scheme where a bright color represents a high correlation (1-white), and a dark color represents low correlation (0-black). Amari errors are reported under each correlation matrix. We also present the discrepancy between the recovered and true sources computed as the sum of the absolute value of the off-diagonal elements of the correlation matrix. A lower discrepancy (Cor disc) indicates better performance. The cICA-LSP has the smallest Amari error and correlation discrepancy among the compared methods.

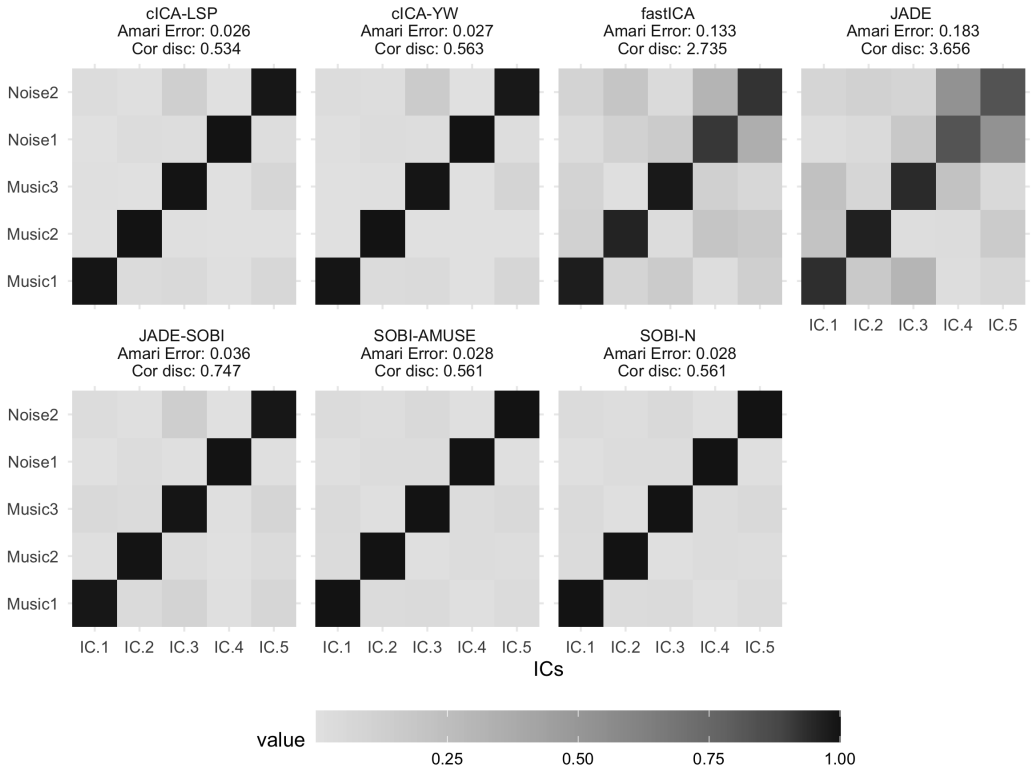


FIGURE 3 Each panel represents a five-by-five correlation matrix, and each entry is colored with a gray color scheme where a dark color represents a high correlation (1-black), and a bright color represents low correlation (0-light gray). Both cICA-LSP and cICA-YW perform better than the other two marginal density-based ICA algorithms in terms of the correlation matrix, and cICA-LSP has the smallest Amari error and correlation discrepancy.

4 | EEG DATA EXAMPLE

EEG signals often include artifacts that do not originate from the brain. The sources of artifacts include power line artifacts (50 or 60 Hz), muscle artifacts, and eye movement. The power line artifact can often be removed by low-pass filtering. Other artifacts can be separated from the brain signals through ICA. Example data is downloaded through the link that the EEGUtils package provides (<https://craddm.github.io/eegUtils/articles/eegUtils.html>). The data was recorded at 1024 Hz using a BioSemi ActiveTwo amplifier and active electrodes and was downsampled to 256 Hz. There were 64 electrodes positioned and named according to the 10-05 international system. Four additional electrodes (EXG1-EXG4) were placed around the eyes to record eye movements, and two further reference electrodes were placed on the left and right mastoids (EXG5 and EXG6). EXG7 and EXG8 are empty channels with no electrodes attached.

As a part of preprocessing, the data was referenced to a common average calculated from all the electrodes after removing the empty channels (EXG7 and EXG8). For reference, the eye movement channels (EXG1-EXG4) were not included in the computing average. Then, we performed Finite Impulse Response (FIR) filtering with a high-pass filter at .1 Hz and a low-pass filter at 40 Hz. Data were epoched around the onset of a visual target on the left and right of fixation. We corrected the baseline using the average time points from -.1 to 0 seconds from the stimulus onsets and limited the range from -.1 to .4 seconds around the stimulus onsets. To run ICA, we included the 64 electrodes and did not include EXG1-EXG6 to focus on the neural signals. The parallel analysis [44] estimated the dimension of ICs as 29. The cICA-LSP and SOBI extracted 29 independent components (Figures 9 and 8 in Appendix). We identified the noise artifacts as the ICs that eye movement (EXG1-EXG4) or mastoid signals (EXG5-6) explained more than 13% of the variance, which is equivalent to medium effect size (Cohen's $f^2=0.15$).

The cICA-LSP identified IC 4 ($R^2 = 0.182$), 10 ($R^2 = 0.136$), 9 ($R^2 = 0.135$), and 1 ($R^2 = 0.131$) as noise artifacts. Those four components explained 29.56% of the total variance of the EEG data, where each of them explained 5.95%, 3.64%, 3.75%, and 16.22% of the total variance, respectively. The SOBI identified IC 1 ($R^2 = 0.183$) and 5 ($R^2 = 0.153$) as the noise artifacts, which explained 17.37% (13.36% and 4.01%, respectively) of the variance of the EEG data. Figures 4 and 5 show the noise artifacts' average ERP and the corresponding topological maps. Figure 6 shows the average ERP before and after artifact removal at the three electrodes located in the midline (Cz, Fz, and Pz) for illustration. The noise artifacts were removed in Fz and Pz, while the signals were similar in Cz. The average ERP at 64 electrodes showed that ICA-based artifact identification removed the large variation toward the tailing signals (Figure 10 in Appendix). After artifact removal, cICA and SOBI seem to have similar effects, while cICA identified more noise artifacts.

5 | CONSISTENCY AND RATE OF CONVERGENCE

In this section, we report the theoretical results of cICA-LSP. We note that [27] investigated the theoretical performance of the Whittle likelihood-based ICA when the source spectral density can be modeled with finite-dimensional parameters. Here we consider more general cases where the sources with mixed spectra, which finite-dimensional parameters may not effectively model.

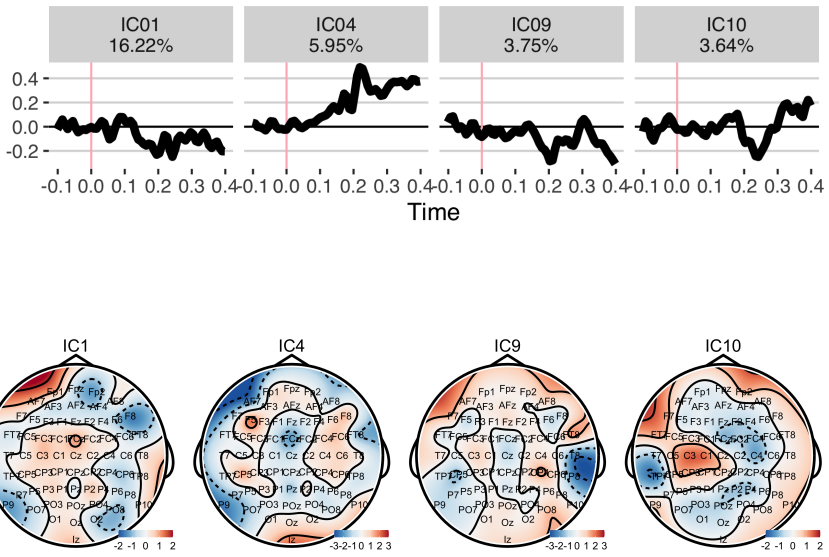


FIGURE 4 Topography maps of the four independent components identified as noise artifacts by cICA-LSP. ICs 1, 4, 9, and 10.

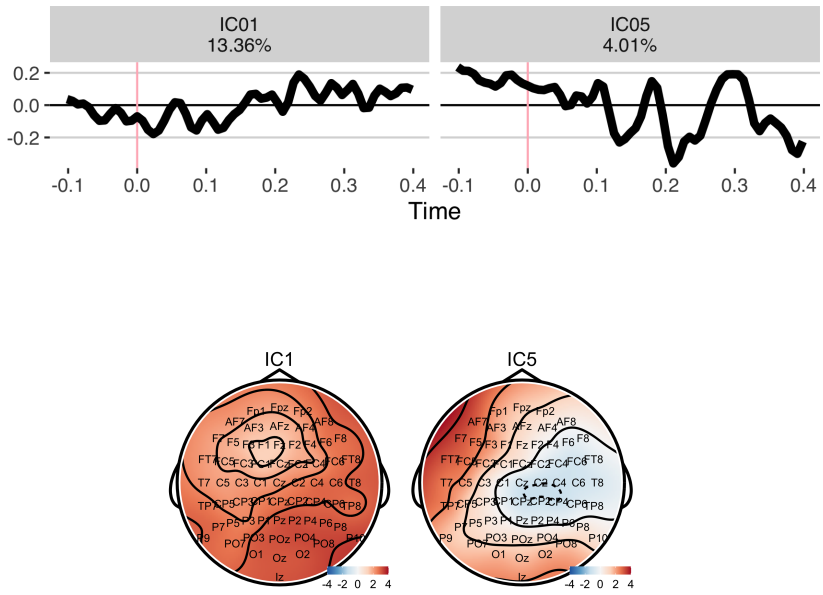


FIGURE 5 Topography maps of the two independent components identified as noise artifacts by SOBI.

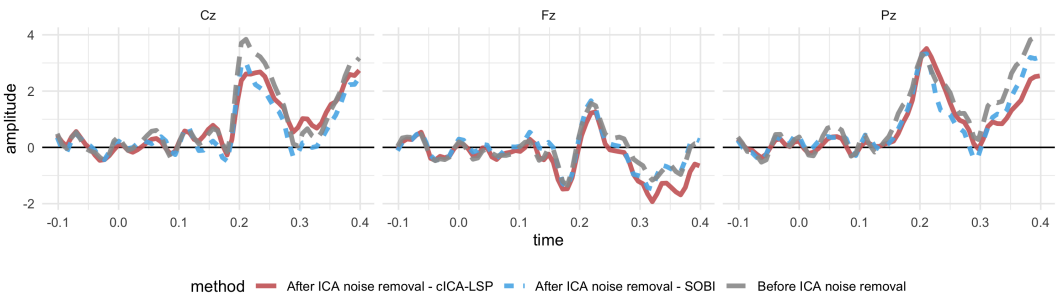


FIGURE 6 Average ERP before and after artifact removal at Cz, Fz and Pz.

5.1 | Statement of the Results

For each $j \in \{1, \dots, M\}$, consider a linear process $\{S_j(t)\}$ is a linear process,

$$S_j(t) = \sum_{k=-\infty}^{\infty} a_{j,k} Z_j(t-k), \quad Z_j(t) \sim i.i.d.(0, \sigma_j^2),$$

with spectral density function

$$f_j(\lambda) = \frac{\sigma_j^2}{2\pi} \left| \sum_{k=-\infty}^{\infty} a_{j,k} \exp(-ik\lambda) \right|^2, \quad -\pi \leq \lambda \leq \pi.$$

Definition A function f on $[0, \pi]$ is said to satisfy *Hölder condition* with exponent γ if there is a positive number c such that $|f(x) - f(x_0)| \leq c \|x - x_0\|^\gamma$ for $x, x_0 \in [0, \pi]$.

Definition Let m be a nonnegative integer and set $p = m + \gamma$. A function f is said to be p -smooth if f is m times differentiable on $[0, \pi]$, and $f^{(m)}$ satisfies a Hölder condition with exponent γ .

The following condition ensures the spectral density functions of each source, $f_j, j \in \{1, \dots, M\}$, are p -smooth.

Condition 1 For each j , Z_j is white noise with finite moment and

$$\sum_k |a_{j,k}| |k|^p < \infty, \quad p > \frac{1}{2}.$$

The following condition ensures that the logarithm of spectral density functions, $\varphi_j = \log f_j$, are bounded. This covers a wide variety of practical spectral densities, including AR or ARMA or the harmonic processes mixed with white noise as described in Examples 3.1 and 3.2.

Condition 2 The power spectrum $f_j(\cdot), j = 1, \dots, M$, are bounded away from zero.

The following condition on the specification of the number of knots K is required for the desirable rate of convergence of the spline-based estimates of the power spectral densities.

Condition 3 For each $j \in \{1, \dots, M\}$, $K_j = O(K)$, where $K^2 = o\left(T^{1-\epsilon}\right)$ for some $\epsilon > 0$.

To address permutation and scale ambiguity in ICA, several authors have used the idea of equivalence class [20, 45, 46, 27]: two matrices \mathbf{W} and $\widetilde{\mathbf{W}}$ are equivalent, denoted as $\mathbf{W} \sim \widetilde{\mathbf{W}}$, if $\widetilde{\mathbf{W}} = (\mathbf{PD})^{-1} \mathbf{W}$ for some permutation matrix \mathbf{P} and a full-rank diagonal matrix \mathbf{D} . Given an equivalence class, the unidentifiability issue can be resolved by choosing a representative of the class according to some identifiability conditions proposed by [20]. A full-rank matrix \mathbf{W} satisfies the following conditions:

1. $\mathbf{W}_1 < \dots < \mathbf{W}_M$ where \mathbf{W}_j is the j th row of \mathbf{W} and we define $<$ as for $\forall \mathbf{a}, \mathbf{b} \in \mathbb{R}^M$ iff there exists $k \in \{1, \dots, M\}$ such that k th element of \mathbf{a} is smaller than that of \mathbf{b} and other element before k th are equal.
2. $\|\mathbf{W}_j\| = 1$ for $j \in \{1, \dots, M\}$.
3. $\max_{1 \leq k \leq M} W_{jk} = \max_{1 \leq k \leq M} |W_{jk}|$ for $j \in \{1, \dots, M\}$.

The following theorems show the consistency and the rate of convergence of the cICA-LSP estimate.

Theorem 1 Let $\widehat{\mathbf{W}}$ be the cICA-LSP estimator and \mathbf{W}_0 be a true unmixing matrix. Under conditions 1-3 and the identifiability condition, $\widehat{\mathbf{W}}$ is consistent.

$$\|\widehat{\mathbf{W}} - \mathbf{W}_0\|_F = o_P(1).$$

Corollary 2 Under the same condition of Theorem 1, the nuisance functions are also consistent.

$$\|\hat{\varphi}_j - \varphi\| = O_P\left(\sqrt{K/T} + K^{-\rho}\right), \quad j \in \{1, \dots, M\}.$$

Theorem 3 Let $\widehat{\mathbf{W}}$ be a nonparametric-colorICA estimator and \mathbf{W}_0 be a true unmixing matrix. Then,

$$\|\widehat{\mathbf{W}} - \mathbf{W}_0\|_F = O_P(T^{-1/2}).$$

5.2 | Proofs

The outline of results is as follows: First, we show the consistency and convergence rate of the Whittle likelihood estimate when the unmixing matrix is orthogonal. To ensure identifiability, we restrict the unmixing matrix to the properly ordered space as [20]. Next, we extend the results to the full rank matrices satisfying the identifiability condition.

Lemma 4 The expected value of the periodogram of \mathbf{S} is $\text{diag}_j\{f_j(r)\} + O(T^{-1})$.

Proof The expectation of the periodogram is given as

$$\begin{aligned} \mathbb{E}\tilde{f}(r, \mathbf{S}) &= \frac{1}{2\pi T} \mathbb{E} \left(\sum_{t=1}^{T-1} \mathbf{S}(t) \exp(-irt) \right) \left(\sum_{t=1}^{T-1} \mathbf{S}(t) \exp(-irt) \right)^* \\ &= \frac{1}{2\pi T} \sum_{t_1=0, t_2=0}^{T-1} \text{diag}_j\{\mathbb{E}S_j(t_1)S_j(t_2)\} \exp(-ir(t_1 - t_2)). \end{aligned}$$

For each j , we have

$$\frac{1}{2\pi T} \sum_{t_1=0, t_2=0}^{T-1} \{\mathbb{E}S_j(t_1)S_j(t_2)\} \exp(-ir(t_1 - t_2)) = \sum_{u=-T+1}^{T-1} \frac{T-|u|}{2\pi T} \gamma_j(u) \exp\{-iru\}.$$

By Condition 1, we have

$$\begin{aligned} &\left| f_j(r) - \frac{1}{2\pi T} \sum_{t_1=0, t_2=0}^{T-1} \{\mathbb{E}S_j(t_1)S_j(t_2)\} \exp(-ir(t_1 - t_2)) \right| \\ &\leq \frac{1}{2\pi} \sum_{|u| \geq T} \gamma_j(u) \exp\{-iru\} + \frac{1}{2\pi} \sum_{|u| \leq T-1} \frac{|u|}{T} \gamma_j(u) \exp\{-iru\} \\ &\leq \frac{1}{2\pi} \sum_{|u| \geq T} \frac{|u|}{T} \gamma_j(u) \exp\{-iru\} + \frac{1}{2\pi} \sum_{|u| \leq T-1} \frac{|u|}{T} \gamma_j(u) \exp\{-iru\} = O(T^{-1}), \quad (11) \end{aligned}$$

and the desired results hold.

Denote the true unmixing matrix as \mathbf{W}_0 . From Lemma 4, the expected value of the Whittle likelihood is give by

$$\begin{aligned} E\mathcal{L}_T(\mathbf{W}, \beta) &= -\frac{1}{[T/2]} \sum_{j=1}^M \sum_{k=1}^{[T/2]} \left\{ \frac{\mathbf{e}_j^\top \mathbf{U} \mathbf{F}_S(r_k) \mathbf{U}^\top \mathbf{e}_j}{\exp\{\mathbf{g}_j(r_k; \beta_j)\}} + \mathbf{g}_j(r_k; \beta_j) \right\} \\ &\quad + T \ln |\det \mathbf{W}| + O(T^{-1}), \end{aligned} \quad (12)$$

where $\mathbf{U} = \mathbf{W}\mathbf{W}_0^{-1}$. Since we restrict \mathbf{W} to orthogonal matrices, we omit the term $\ln |\det \mathbf{W}|$ rest of this paper. Let the asymptotic expected Whittle log-likelihood written as

$$\Lambda_T(\mathbf{W}, \beta) = -\frac{1}{[T/2]} \sum_{j=1}^M \sum_{k=1}^{[T/2]} \left\{ \frac{\mathbf{e}_j^\top \mathbf{U} \mathbf{F}_S(r_k) \mathbf{U}^\top \mathbf{e}_j}{\exp\{\mathbf{g}_j(r_k; \beta_j)\}} + \mathbf{g}_j(r_k; \beta_j) \right\}, \quad (13)$$

By Jensen's inequality and orthogonality of \mathbf{W}_0 and \mathbf{W} , $\Lambda_T(\mathbf{W}, \beta)$ is bounded by $\Lambda_T(\mathbf{W}_0, \varphi)$:

$$\begin{aligned} \Lambda_T(\mathbf{W}, \beta) &\leq -\frac{1}{[T/2]} \sum_{j=1}^M \sum_{k=1}^{[T/2]} \left\{ 1 + \sum_{l=1}^M \log U_{jl}^2 f_l(r_k) \right\} \\ &\leq -\frac{1}{[T/2]} \sum_{k=1}^{[T/2]} \sum_{l=1}^M \left\{ 1 + \sum_{j=1}^M U_{jl}^2 \log f_l(r_k) \right\} = \Lambda_T(\mathbf{W}_0, \varphi). \end{aligned} \quad (14)$$

5.2.1 | Bias

For a given orthogonal matrix \mathbf{W} , write $\varphi_j^W = \log(\sum_{m=1}^M U_{jm}^2 f_m)$, where $\mathbf{U} = \mathbf{W}\mathbf{W}_0^{-1}$.

Lemma 5 *Let ϵ be a positive constant. There exist positive constants c_1 and c_2 such that*

$$\|\varphi_j^W - \varphi_j\|^2 \leq c_1 \|\mathbf{W} - \mathbf{W}_0\|_F^2, \text{ and } \|\varphi_j^W - \varphi_j\|_\infty \leq c_2 \|\mathbf{W} - \mathbf{W}_0\|_F^2,$$

for ϵ small enough and any orthogonal matrix \mathbf{W} satisfying $\|\mathbf{W} - \mathbf{W}_0\|_F \leq \epsilon$.

Proof For a give $\epsilon > 0$, let \mathbf{W} be close to \mathbf{W}_0 such that $\|\mathbf{W} - \mathbf{W}_0\|_F < \epsilon$. Let the difference matrix δ satisfy $\mathbf{U} = \mathbf{W}\mathbf{W}_0^{-1} = \mathbf{I} + \delta$. This leads $\mathbf{W} = \mathbf{W}_0 + \delta\mathbf{W}_0$. Then, we have $M - \epsilon \leq \text{tr}(\mathbf{U}) \leq M$ and $-\epsilon^2/2 \leq \text{tr}(\delta) \leq 0$. Since \mathbf{U} is orthogonal, we have $-2\text{tr}(\delta) = \sum_{j,m} \delta_{jm}^2$. Thus, the sum of squares of the difference matrix is bounded as $0 \leq \sum_{j,m} \delta_{jm}^2 \leq \epsilon^2$. Note that from the orthogonality condition, all the diagonal elements of δ have negative value.¹

For each $j = 1, \dots, M$,

$$\begin{aligned} \|\varphi_j^W - \varphi_j\|^2 &= \int \left(\log \left(\frac{\sum_{m=1}^M U_{jm}^2 f_m(r)}{f_j(r)} \right) \right)^2 dr \\ &= \int \left(\log \left(1 + 2\delta_{jj} + \frac{\sum_{m=1}^M \delta_{jm}^2 f_m(r)}{f_j(r)} \right) \right)^2 dr \end{aligned} \quad (15)$$

¹Assume that there is at least one j such that $\delta_{jj} > 0$. Since \mathbf{U} is orthogonal, $\|\mathbf{U}\mathbf{e}_j\|^2 = 1 + 2\delta_{jj} + \sum_{m=1}^M \delta_{jm}^2 = 1$. The equality holds only if $\delta_{jj} = 0$, which contradicts the assumption.

Then the righthand side of (15) is bounded by

$$\begin{aligned}
 (15) &\leq \int \left| 2\delta_{jj} + \sum_{m=1} \delta_{jm}^2 \frac{f_m(r)}{f_j(r)} \right| dr \leq b_1 \int 2|\delta_{jj}| + \left(\frac{\sum_{m=1}^M \delta_{jm}^2 f_m(r)}{f_j(r)} \right)^2 dr \\
 &\leq b_1 \left(-2 \sum_{j=1}^M \delta_{jj} + b_2 \sum_{j=1}^M \delta_{jm}^2 \right) \leq b_1 (\epsilon^2 + b_2 \epsilon^2) = b_1 (1 + b_2) \|\mathbf{W} - \mathbf{W}_0\|_F^2,
 \end{aligned} \tag{16}$$

where b_1 is a positive constant and $b_2 = \frac{1}{2\pi} \max_{m,j} \sup_r \frac{f_m(r)}{f_j(r)}$.

Similarly,

$$\begin{aligned}
 \|\varphi_j^W - \varphi_j\|_\infty &= \int \sup_r \left| \ln \left(1 + 2\delta_{jj} + \frac{\sum_{m=1}^M \delta_{jm}^2 f_m(r)}{f_j(r)} \right) \right| dr \\
 &\leq b_3 \int 2|\delta_{jj}| + \sum_{m=1}^M \delta_{jm}^2 \sup_r \frac{f_m(r)}{f_j(r)} dr \\
 &\leq b_3 \left(-2 \sum_{j=1}^M \delta_{jj} \right) + b_4 \sum_{j=1}^M \delta_{jm}^2 \leq (b_3 + b_4) \|\mathbf{W} - \mathbf{W}_0\|_F^2.
 \end{aligned} \tag{17}$$

Thus, the desired results hold.

Write $\hat{\beta}^W = \arg \max_{(\beta; g(\cdot; \beta_j) \in \mathcal{S}, j=1, \dots, M)} L_T(\mathbf{W}, \beta)$ and $\hat{\varphi}_j^W = g(\cdot; \hat{\beta}_j^W)$. By the Theorem of [47], for any given orthogonal matrix \mathbf{W} , $\hat{\varphi}^W$ is a consistent estimate of φ^W such that

$$\|\hat{\varphi}_j^W - \varphi_j^W\| = O_p \left(\sqrt{\frac{K}{T}} + K^{-p} \right), \quad j = 1, \dots, M.$$

From Lemma 5, if \mathbf{W} is close to \mathbf{W}_0 , for a positive constant c ,

$$\begin{aligned}
 \|\hat{\varphi}_j^W - \varphi_j\| &\leq \underbrace{\|\hat{\varphi}_j^W - \varphi_j^W\|}_{\leq O_p \left(\sqrt{\frac{K}{T}} + K^{-p} \right)} + \underbrace{\|\varphi_j^W - \varphi_j\|}_{\leq c \|\mathbf{W} - \mathbf{W}_0\|_F^2} \\
 &\leq O_p \left(\sqrt{\frac{K}{T}} + K^{-p} \right) + c \|\mathbf{W} - \mathbf{W}_0\|_F^2
 \end{aligned}$$

This indicates that the bias depends on that of $\widehat{\mathbf{W}}$.

Let $\tau_T, T \geq 1$, be positive numbers such that $K\tau_T^2 = O(1)$ and $\frac{1}{T} = o\left(\tau_T^2\right)$.

Lemma 6 Let b_1, b_2 and b_3 be positive constants. There is a positive constant b_4 such that, for T sufficiently large,

$$\Pr \left(|L_T(\mathbf{W}, \mathbf{g}) - L_T(\mathbf{W}^*, \mathbf{g}^*) - \Lambda_T(\mathbf{W}, \mathbf{g}) + \Lambda_T(\mathbf{W}^*, \mathbf{g}^*)| \geq b_1 \tau_T \right) \leq 2 \exp \left(-b_4 T \tau_T^2 \right)$$

for any \mathbf{W} satisfying $\|\mathbf{W} - \mathbf{W}^*\|_F \leq b_2 \tau_T$ and \mathbf{g}_j satisfying $\|\mathbf{g}_j - \mathbf{g}_j^*\|_F \leq b_3 \tau_T$.

Proof By Hoeffding's inequality, for any positive constant $t > 0$, there is a positive constant c such that

$$\begin{aligned} & \Pr \left(\left| L_T(\mathbf{W}, \mathbf{g}) - L_T(\mathbf{W}^*, \mathbf{g}^*) - \Lambda_T(\mathbf{W}, \mathbf{g}) + \Lambda_T(\mathbf{W}^*, \mathbf{g}^*) \right| \geq b_1 \tau_T \right) \\ &= \Pr \left(\exp \left\{ t \left[L_T(\mathbf{W}, \mathbf{g}) - L_T(\mathbf{W}^*, \mathbf{g}^*) - \Lambda_T(\mathbf{W}, \mathbf{g}) + \Lambda_T(\mathbf{W}^*, \mathbf{g}^*) \right] \right\} \geq \exp \{ t b_1 \tau_T \} \right) \\ &\leq 2 \left\{ 1 + t^2 \frac{c}{2T} \right\} \exp \{ -t b_1 \tau_T \} \\ &\leq 2 \exp \left\{ t^2 \frac{c}{2T} - t b_1 \tau_T \right\}. \end{aligned}$$

If we set $t = \frac{T b_1 \tau_T}{c}$, then the desired results hold.

Write $\mathbf{g}_j^{(l)}(\cdot) = \mathbf{g}(\cdot; \beta_j^{(l)})$, for $j = 1, \dots, M$ and $l = 1, 2$.

Lemma 7 Let ϵ, b_1, b_3 and b_2 be positive constants. Then, except on an event with probability tending to zero as $T \rightarrow \infty$,

$$\left| L_T(\mathbf{W}_1, \mathbf{g}^{(1)}) - L_T(\mathbf{W}_2, \mathbf{g}^{(2)}) \right| \leq \epsilon \tau_T$$

for all $\|\mathbf{W}_1 - \mathbf{W}_2\|_F \leq b_1 \tau_T$, $\|\mathbf{g}_j^{(1)} - \mathbf{g}_j^{(2)}\|_\infty \leq b_2 \tau_T$, $\|\mathbf{g}_j^{(1)}\|_\infty \leq b_3$ and $\|\mathbf{g}_j^{(2)}\|_\infty \leq b_3$.

Proof Write $\mathbf{G}_l(r_k) = \text{diag}_{j=1, \dots, M} \{ \mathbf{g}_j^{(l)}(r_k) \}$, $l = 1, 2$.

$$\begin{aligned} & \left| L_T(\mathbf{W}_1, \mathbf{g}^{(1)}) - L_T(\mathbf{W}_2, \mathbf{g}^{(2)}) \right| \\ &\leq \frac{1}{2T} \sum_{j,k} \left| \text{tr} \left(\tilde{\mathbf{f}}(r_k; \mathbf{X}) \left\{ \mathbf{W}_1^\top \mathbf{G}_1^{-1}(r_k) \mathbf{W}_1 - \mathbf{W}_2^\top \mathbf{G}_2^{-1}(r_k) \mathbf{W}_2 \right\} \right) \right| + \frac{1}{2T} \sum_{j,k} \left| \mathbf{g}_j^{(1)}(r_k) - \mathbf{g}_j^{(2)}(r_k) \right| \\ &\leq \frac{1}{2T} \sum_{j,k} \left| \text{tr} \left(\tilde{\mathbf{f}}(r_k; \mathbf{X}) \left\{ \mathbf{W}_1^\top \mathbf{G}_1^{-1}(r_k) \mathbf{W}_1 - \mathbf{W}_1^\top \mathbf{G}_2^{-1}(r_k) \mathbf{W}_1 \right\} \right) \right| \\ &\quad + \frac{1}{2T} \sum_{j,k} \left| \text{tr} \left(\tilde{\mathbf{f}}(r_k; \mathbf{X}) \left\{ \mathbf{W}_1^\top \mathbf{G}_2^{-1}(r_k) \mathbf{W}_1 - \mathbf{W}_1^\top \mathbf{G}_2^{-1}(r_k) \mathbf{W}_2 \right\} \right) \right| \\ &\quad + \frac{1}{2T} \sum_{j,k} \left| \text{tr} \left(\tilde{\mathbf{f}}(r_k; \mathbf{X}) \left\{ \mathbf{W}_1^\top \mathbf{G}_2^{-1}(r_k) \mathbf{W}_2 - \mathbf{W}_2^\top \mathbf{G}_2^{-1}(r_k) \mathbf{W}_2 \right\} \right) \right| + M b_2 \tau_T \\ &= O_p(1) (b_2 + 2b_1 b_3) \tau_T \end{aligned}$$

Proof of Theorem 1 Write $\theta = (\text{vec}(\mathbf{W})^\top, \beta^\top)^\top$. From Lemmas 6 and 7, except on an event whose probability tends to zero as $T \rightarrow \infty$, $L_T(\mathbf{W}^{(1)}, \mathbf{g}^{(1)}) < L_T(\mathbf{W}^*, \mathbf{g}^*)$ for $\|\mathbf{W}^{(1)} - \mathbf{W}^*\|_F = b_1 \tau_T$ and $\|\mathbf{g}_j^{(1)} - \mathbf{g}_j^*\| = b_2 \tau_T$. For fixed constants b_1 and b_2 , denote an open ball at θ with radius τ_T as $N(\theta; \tau_T) = \{ \theta^{(1)} : \|\mathbf{W}^{(1)} - \mathbf{W}^*\|_F \leq b_1 \tau_T, \|\mathbf{g}_j^{(1)} - \mathbf{g}_j^*\| \leq b_2 \tau_T \}$. Then we have

$$\lim_{T \rightarrow \infty} \Pr \left\{ \sup_{\theta \in N(\theta_1; \tau_T)} L_T(\mathbf{W}, \mathbf{g}) - L_T(\mathbf{W}^*, \mathbf{g}^*) < 0 \right\} = 1. \quad (18)$$

Let $B = \{ (\mathbf{W}, \beta) : \|\mathbf{W} - \mathbf{W}_0\|_F \geq b_1 \tau_T, \|\mathbf{g}_j - \mathbf{g}_j^*\| \geq b_2 \tau_T \}$. Since B is compact, there exists a collection of finite number of open coverings: $\{ N(\theta_p; \delta_p) : p = 1, \dots, P \}$.

By (18) and finite number P , we have

$$\lim_{T \rightarrow \infty} \Pr \left\{ \sup_{\theta \in \cup_{\rho=1}^P N(\theta_\rho; \delta_\rho)} L_T(\mathbf{W}, \mathbf{g}) - L_T(\mathbf{W}^*, \mathbf{g}^*) < 0 \right\} = 1,$$

thus,

$$\lim_{T \rightarrow \infty} \Pr \left\{ \sup_{\theta} L_T(\mathbf{W}, \mathbf{g}) = \sup_{\theta \in N(\theta^*; \tau_T)} L_T(\mathbf{W}, \mathbf{g}) \right\} = 1,$$

Therefore, $\|\widehat{\mathbf{W}} - \mathbf{W}^*\| = o_P(\tau_T) = o_P(1)$ and $\|\hat{\mathbf{g}}_j - \mathbf{g}_j^*\| = o_P(\tau_T)$. From (13), the definition of \mathbf{W}^* and \mathbf{g}^* and Lemma 2 from [47],

$$\begin{aligned} 0 &\leq \Lambda_T(\mathbf{W}^*, \mathbf{g}^*) - \Lambda_T(\mathbf{W}_0, \mathbf{g}^{W_0}) \leq \Lambda_T(\mathbf{W}_0, \varphi) - \Lambda_T(\mathbf{W}_0, \mathbf{g}^{W_0}) \\ &\leq c \sum_{j=1}^M \|\varphi_j - \mathbf{g}^{W_0}\| = O(K^{-2p}). \end{aligned} \quad (19)$$

Let $\dot{\Lambda}_T(\theta) = \frac{\partial \Lambda_T(\theta)}{\partial \theta}$. We can write $\int_0^1 \frac{\partial}{\partial u} \Lambda_T(\theta^* + u(\theta_0 - \theta^*)) du = \Lambda_T(\mathbf{W}^*, \mathbf{g}^*) - \Lambda_T(\mathbf{W}_0, \mathbf{g}^{W_0})$. This can further be written as $\mathbf{D}(\theta^* - \theta_0) = \Lambda_T(\mathbf{W}^*, \mathbf{g}^*) - \Lambda_T(\mathbf{W}_0, \mathbf{g}^{W_0})$, where \mathbf{D} is given by $\mathbf{D} = \int_0^1 \dot{\Lambda}_T(\theta^* + u(\theta_0 - \theta^*)) du$. Since \mathbf{D} is bounded, we have $\|\theta^* - \theta_0\| = O(K^{-2p})$.

Thus, $\|\widehat{\mathbf{W}} - \mathbf{W}_0\| = o_P(1)$ and $\|\hat{\mathbf{g}}_j - \varphi_j\| = o_P(1)$.

5.3 | Variance

Let $\dot{L}_T(\theta)$ denote the score at θ of $(M^2 + MK)$ -dimensional vector with entries $\frac{\partial L_T(\theta)}{\partial \theta_j}$:

$$\begin{aligned} \frac{\partial L(\theta)}{\partial \mathbf{W}_j} &= -2 \frac{1}{[T/2]} \sum_k \tilde{\mathbf{f}}(r_k; \mathbf{X}) \mathbf{W}_j \exp\{-\mathbf{g}_j(r_k; \beta_j)\} \\ \frac{\partial L(\theta)}{\partial \beta_j} &= \frac{1}{[T/2]} \sum_k \text{tr}(\mathbf{W} \tilde{\mathbf{f}}(r_k; \mathbf{X}) \mathbf{W}^\top) \exp\{-\mathbf{g}_j(r_k; \beta_j)\} \mathbf{B}_j(r_k) - \frac{1}{[T/2]} \sum_k \mathbf{B}_j(r_k). \end{aligned} \quad (20)$$

Let $\mathbf{H}_T(\theta)$ denote the Hessian at θ ; that is, the $(M^2 + \sum_j K_j) \times (M^2 + \sum_j K_j)$ matrix with entries $\frac{\partial^2 L_T(\theta)}{\partial \theta_j \partial \theta_k}$:

$$\begin{aligned} \frac{\partial^2 L(\theta)}{\partial \mathbf{W}_j \partial \mathbf{W}_k} &= -\frac{2}{[T/2]} \sum_k \delta_{j-k} \tilde{\mathbf{f}}(r_k; \mathbf{X}) \exp\{-\mathbf{g}_j(r_k; \beta_j)\} \\ \frac{\partial^2 L(\theta)}{\partial \mathbf{W}_j \partial \beta_k} &= \frac{2}{[T/2]} \sum_k \delta_{j-k} \left(\tilde{\mathbf{f}}(r_k; \mathbf{X}) \mathbf{W}_j \right) \exp\{-\mathbf{g}_j(r_k; \beta_j)\} \mathbf{B}_j(r_k) \\ \frac{\partial^2 L(\theta)}{\partial \beta_j \partial \beta_k} &= \frac{1}{[T/2]} \sum_k \delta_{j-k} \text{tr}(\mathbf{W} \tilde{\mathbf{f}}(r_k; \mathbf{X}) \mathbf{W}^\top) \exp\{-\mathbf{g}_j(r_k; \beta_j)\} \mathbf{B}_j(r_k) \mathbf{B}_j(r_k)^\top. \end{aligned} \quad (21)$$

Then, we have

$$\int_0^1 \frac{d}{du} \dot{L}_T(\theta^* + u(\hat{\theta} - \theta^*)) du = \dot{L}_T(\hat{\theta}) - \dot{L}_T(\theta^*). \quad (22)$$

Define a $(M^2 + MK) \times (M^2 + MK)$ matrix $\mathbf{D} = \int_0^1 \mathbf{H}_T(\boldsymbol{\theta}^* + u(\hat{\boldsymbol{\theta}} - \boldsymbol{\theta}^*)) du$. Then (22) can be written as $\mathbf{D}(\hat{\boldsymbol{\theta}} - \boldsymbol{\theta}^*) = \dot{L}_T(\hat{\boldsymbol{\theta}}) - \dot{L}_T(\boldsymbol{\theta}^*)$. Since $(\hat{\boldsymbol{\theta}} - \boldsymbol{\theta}^*)^\top \dot{L}_T(\hat{\boldsymbol{\theta}}) = 0$ and $(\hat{\boldsymbol{\theta}} - \boldsymbol{\theta}^*)^\top \mathbf{E} \dot{L}_T(\hat{\boldsymbol{\theta}}) = 0$, we have

$$(\hat{\boldsymbol{\theta}} - \boldsymbol{\theta}^*)^\top \mathbf{D}(\hat{\boldsymbol{\theta}} - \boldsymbol{\theta}^*)^\top = -(\hat{\boldsymbol{\theta}} - \boldsymbol{\theta}^*)^\top (\dot{L}_T(\boldsymbol{\theta}^*) - \mathbf{E} \dot{L}_T(\boldsymbol{\theta}^*)). \quad (23)$$

Lemma 8 Under Condition 1, we have

$$|\dot{L}_T(\boldsymbol{\theta}^*) - \mathbf{E} \dot{L}_T(\boldsymbol{\theta}^*)|^2 = O_P\left(\frac{1}{T}\right).$$

Lemma 9 There exists a positive constant c such that

$$(\hat{\boldsymbol{\theta}} - \boldsymbol{\theta}^*)^\top \mathbf{D}(\hat{\boldsymbol{\theta}} - \boldsymbol{\theta}^*)^\top \leq \frac{cK^{-1}}{T} \|\hat{\boldsymbol{\theta}} - \boldsymbol{\theta}^*\|^2,$$

except on an event whose probability tends to zero as $T \rightarrow \infty$.

Proof Write $\mathbf{a} = \hat{\boldsymbol{\theta}} - \boldsymbol{\theta}^*$, $\mathbf{a}^W = (\text{vec}(\widehat{\mathbf{W}}) - \text{vec}(\mathbf{W}^*))$, $\mathbf{a}_j^\beta = (\hat{\beta}_j - \beta_j^*)$. For any $\boldsymbol{\theta}$,

$$\mathbf{a}^\top \mathbf{H}_T(\boldsymbol{\theta}) \mathbf{a} = - \sum_{j=1}^M \frac{2}{[T/2]} \mathbf{a}_j^{W^\top} \sum_k \text{Re} \bar{\mathbf{f}}(r_k; \mathbf{X}) \exp\{-\beta_j^\top \mathbf{B}_j(r_k)\} \mathbf{a}_j^W \quad (24)$$

$$+ 2 \sum_{j=1}^M \frac{2}{[T/2]} \mathbf{a}_j^{W^\top} \sum_k \text{Re} \bar{\mathbf{f}}(r_k; \mathbf{X}) \mathbf{W}_j^\top \exp\{-\beta_j^\top \mathbf{B}_j(r_k)\} \mathbf{B}_j^\top(r_k) \mathbf{a}_j^\beta \quad (25)$$

$$- \sum_{j=1}^M \frac{1}{[T/2]} \mathbf{a}_j^{\beta^\top} \text{tr}(\mathbf{W} \bar{\mathbf{f}}(r_k; \mathbf{X}) \mathbf{W}^\top) \exp\{-g_j(r_k; \beta_j)\} \mathbf{B}_j(r_k) \mathbf{B}_j(r_k)^\top \mathbf{a}_j^\beta \quad (26)$$

From the asymptotic distribution of the periodogram, we have

$$\frac{2}{[T/2]} \sum_k \text{Re} \bar{\mathbf{f}}(r_k; \mathbf{X}) \exp\{-\beta_j^\top \mathbf{B}_j(r_k)\} = O_P(T^{-1/2}). \quad (27)$$

Then there is a positive constant c_1 , such that

$$\sum_{j=1}^M \frac{2}{[T/2]} \mathbf{a}_j^{W^\top} \sum_k \text{Re} \bar{\mathbf{f}}(r_k; \mathbf{X}) \exp\{-\beta_j^\top \mathbf{B}_j(r_k)\} \mathbf{a}_j^W \geq c_1 \|\mathbf{a}^W\|^2 \geq c_1 K^{-1} \|\mathbf{a}^W\|^2.$$

From the Lemma 6 in [47], there is a positive constant c_2 such that

$$\sum_{j=1}^M \frac{1}{[T/2]} \text{tr}(\mathbf{W} \bar{\mathbf{f}}(r_k; \mathbf{X}) \mathbf{W}^\top) \exp\{-g_j(r_k; \beta_j)\} \left| (\hat{\beta}_j - \beta_j^*)^\top \mathbf{B}_j(r_k) \right|^2 \geq c_2 K^{-1} \|\hat{\beta}_j - \beta_j^*\|^2.$$

Also, there exists a positive constant c_3 such that

$$\begin{aligned} |(25)| &\leq \sqrt{2} \sum_{j=1}^M \|\mathbf{a}_j^W\| \left\| \frac{2}{[T/2]} \sum_k \text{Re} \bar{\mathbf{f}}(r_k; \mathbf{X}) \mathbf{W}_j^\top \exp\{-\beta_j^\top \mathbf{B}_j(r_k)\} \mathbf{B}_j^\top(r_k) \right\|_F \|\mathbf{a}_j^\beta\| \\ &\leq c_3 \|\mathbf{a}\|^2. \end{aligned}$$

Thus, there exists a positive constant c_4 such that $\mathbf{a}^\top \mathbf{H}_T(\boldsymbol{\theta}) \mathbf{a} \leq -c_4 K^{-1} \|\mathbf{a}\|^2$.

Since

$$|(\hat{\boldsymbol{\theta}} - \boldsymbol{\theta}^*)^\top (\dot{L}_T(\boldsymbol{\theta}^*) - E\dot{L}_T(\boldsymbol{\theta}^*))| \leq |\hat{\boldsymbol{\theta}} - \boldsymbol{\theta}^*| |\dot{L}_T(\boldsymbol{\theta}^*) - E\dot{L}_T(\boldsymbol{\theta}^*)|,$$

and from Lemmas 8–9, we have

$$\|\hat{\boldsymbol{\theta}} - \boldsymbol{\theta}^*\|^2 = O_P(K^2/T), \quad (28)$$

6 | CONCLUSION

This paper proposed a new independent component analysis for the auto-correlated sources with mixed spectra. We derived the Whittle likelihood function to handle autocorrelation. We also employed nonparametric spectral density estimation to model the mixed spectra accurately. Numerical experiments showed superior performance of recovering sources compared to existing ICA methods and supported the theoretical findings. Furthermore, EEG data application demonstrated its effectiveness in applications.

Appendix

| Simulation Results

Figure 7 includes the performance of JADE and fastICA, in addition to those shown in Figure 1. JADE and fastICA performed much worse than the ICA methods account for autocorrelation.

| EEG Data Analysis Results

Here we included the rest of the EEG data analysis results. Figures 8 and 9 show the topography maps, average ERP, and variance explained by component of the 29 ICs obtained by SOBI and cICA-LSP. Figure 10 shows the average ERP before and after artifact removal using SOBI (removing ICs 1 and 5) and cICA-LSP (removing ICs 1, 4, 9 and 10), respectively.

references

- [1] Hyvärinen A, Karhunen J, Oja E. Independent Component Analysis. John Wiley & Sons; 2001.
- [2] Hastie T, Tibshirani R, Friedman JH. The Elements of Statistical Learning: Data Mining, Inference, and Prediction. Second ed. Springer Verlag; 2009.
- [3] Cichocki A, Zdunek R, Phan AH. Nonnegative Matrix and Tensor Factorizations: Applications to Exploratory Multi-way Data Analysis and Blind Source Separation. Wiley; 2009.
- [4] Comon P, Jutten C. Handbook of Blind Source Separation: Independent Component Analysis and Applications. Academic Press; 2010.
- [5] Back AD, Weigend AS. A First Application of Independent Component Analysis to Extracting Structure from Stock Returns. International Journal of Neural Systems 1997;8:473–484.

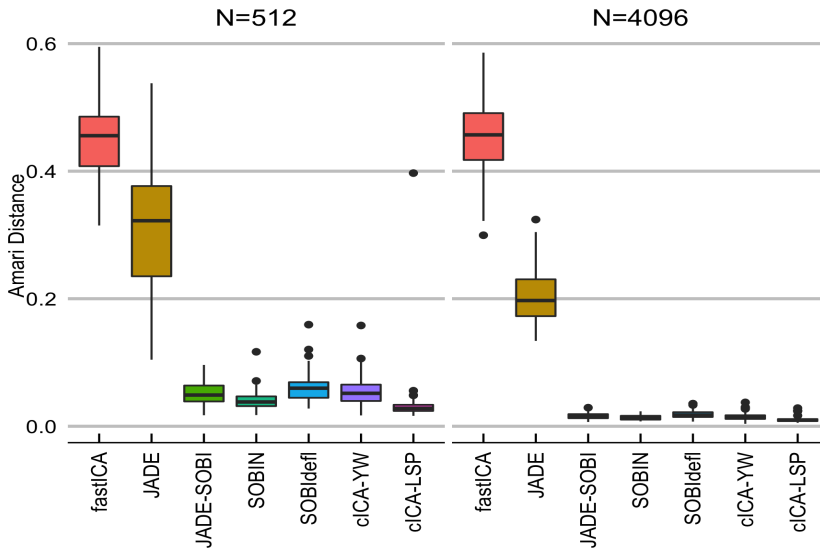


FIGURE 7 Simulation Study I: Full performance comparisons including JADE and fastICA in addition to those presented in Figure 1.

- [6] Calhoun VD, Liu J, Adali T. A Review of Group ICA for fMRI Data and ICA for Joint Inference of Imaging, Genetic, and ERP Data. *NeuroImage* 2009;45(1S1):163–172.
- [7] Makeig S, Onton J. ERP Features and EEG Dynamics: An ICA perspective. In: Luck S, Kappenman E, editors. *Oxford Handbook of Event-related Potential Components* Oxford University Press; 2009.
- [8] Ge Z, Song Z. Process Monitoring Based on Independent Component Analysis-principal Component Analysis (ICA-PCA) and Similarity Factors. *Industrial & Engineering Chemistry Research* 2007;46(7):2054–2063.
- [9] Cardoso JF, Souloumiac A. Blind beamforming for non-Gaussian signals. In: *Radar and Signal Processing*, IEE Proceedings F, vol. 140 IET; 1993. p. 362–370.
- [10] Bell AJ, Sejnowski TJ. An Information-Maximization Approach to Blind Separation and Blind Deconvolution. *Neural Computation* 1995;7(6):1129–1159.
- [11] Lee TW, Girolami M, Sejnowski TJ. Independent Component Analysis Using an Extended Infomax Algorithm for Mixed Subgaussian and Supergaussian Sources. *Neural Computation* 1999;11(2):417–441.
- [12] Vlassis N, Motomura Y. Efficient Source Adaptivity in Independent Component Analysis. *IEEE Transactions on Neural Networks* 2001;12(3):559–566.
- [13] Chen A, Bickel PJ. Efficient Independent Component Analysis. *The Annals of Statistics* 2006;34(6):2825–2855.
- [14] Bach FR, Jordan MI. Kernel Independent Component Analysis. *Journal of Machine Learning Research* 2003;3(1):1–48.
- [15] Boscolo R, Pan H, Roychowdhury V. Independent Component Analysis Based on Nonparametric Density Estimation. *IEEE Transactions on Neural Networks* 2004;15(1):55–65.
- [16] Chen A. Fast Kernel Density Independent Component Analysis. *Independent Component Analysis and Blind Signal Separation* 2006;3889:24–31.

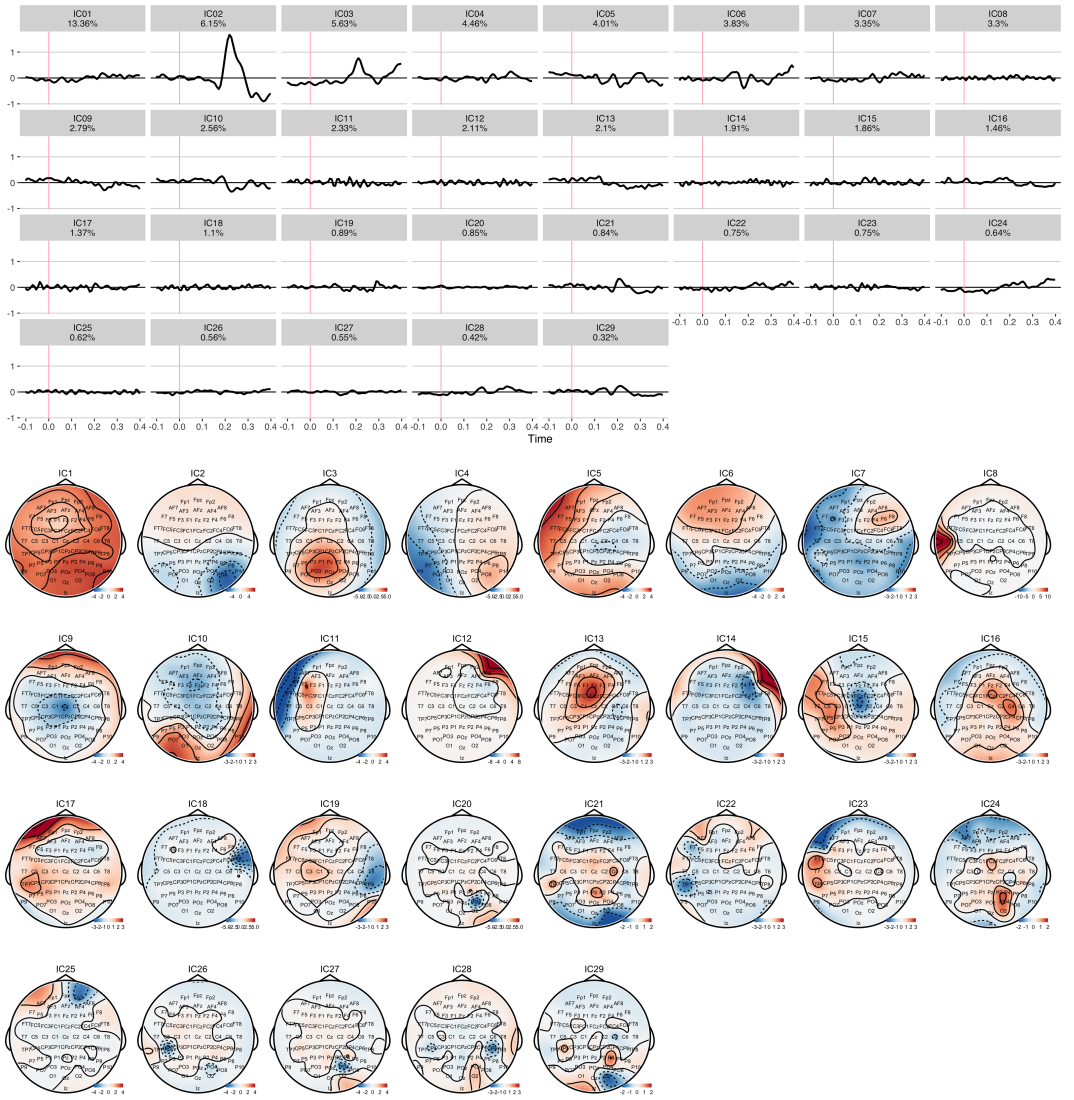


FIGURE 8 Topography maps of the 29 independent components identified by SOBI. ICs 1 and 5 were identified artifacts that are largely related to eye movement and mastoids.

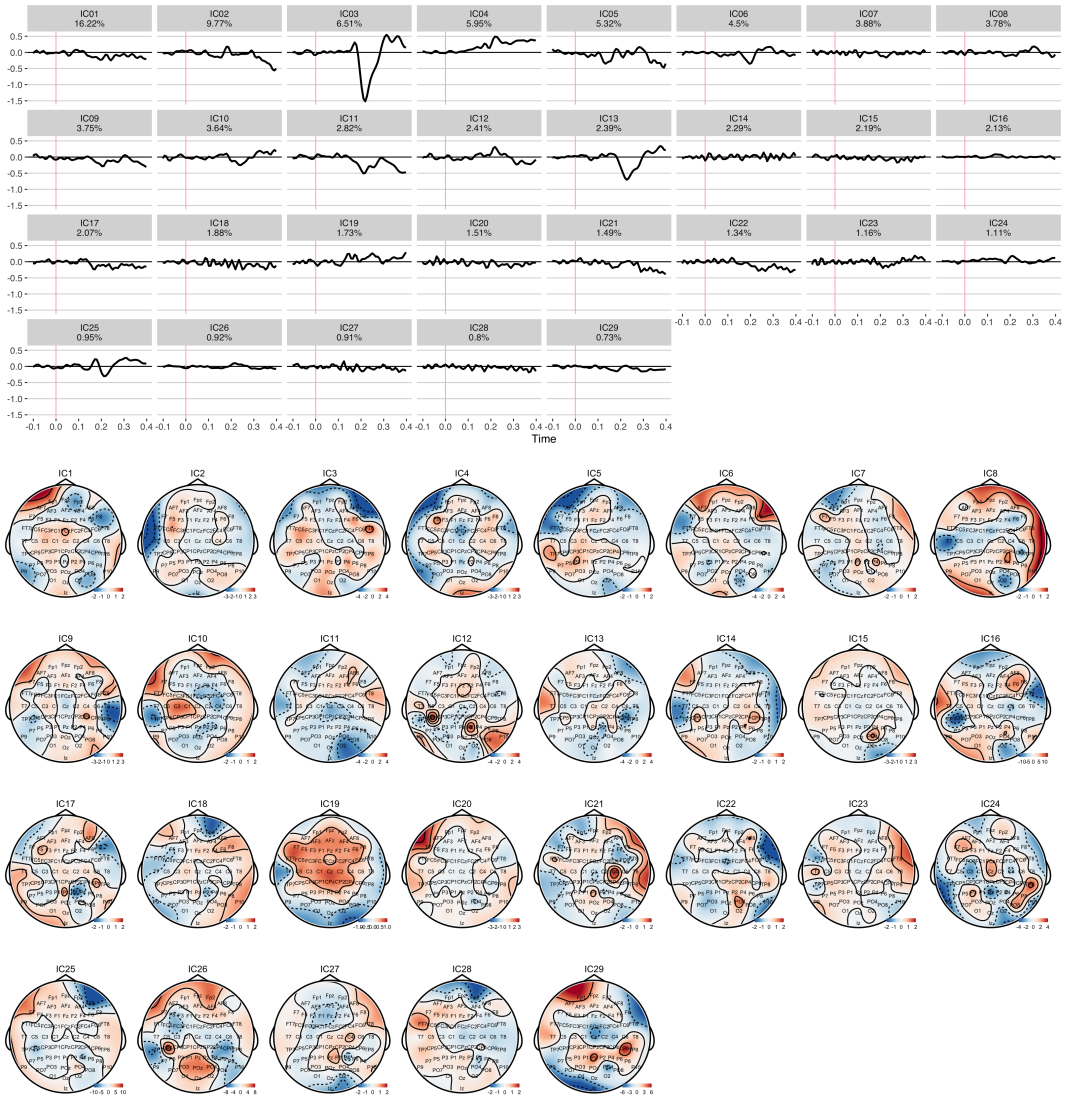


FIGURE 9 Topography maps of the 29 independent components identified by cICA-LSP. ICs 1, 4, 9 and 10 were identified artifacts that are largely related to eye movement.

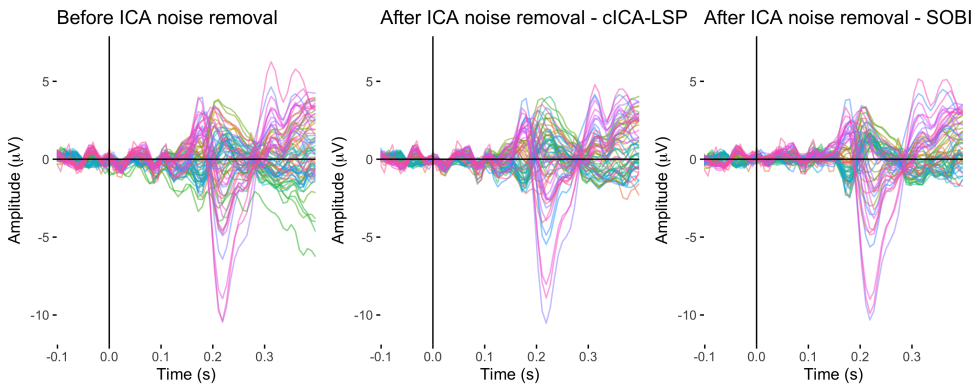


FIGURE 10 Average ERP before and after artifact removal at 64 electrodes using cICA-LSP and SOBI.

- [17] Hastie T, Tibshirani R. Independent Components Analysis Through Product Density Estimation. In: Becker S, Obermayer K, editors. *Advances in Neural Information Processing Systems*, vol. 15 Cambridge, MA: MIT Press; 2003. p. 665–672.
- [18] Kawaguchi A, Truong YK. *Spline Independent Component Analysis*. University of North Carolina at Chapel Hill; 2009.
- [19] Eriksson J, Koivunen V. Characteristic-function-based Independent Component Analysis. *Signal Processing* 2003;83(10):2195–2208.
- [20] Chen A, Bickel P. Consistent Independent Component Analysis and Prewhitening. *IEEE Transactions on Signal Processing* 2005;53(10 Part 1):3625–3632.
- [21] Matteson DS, Tsay RS. *Independent Component Analysis via Distance Covariance*. Cornell University; 2011.
- [22] Matteson DS, Tsay RS. Independent component analysis via distance covariance. *Journal of the American Statistical Association* 2017;112(518):623–637.
- [23] Belouchrani A, Abed-Meraim K, Cardoso JF, Moulines E. A blind source separation technique using second-order statistics. *IEEE Transactions on signal processing* 1997;45(2):434–444.
- [24] Miettinen J, Nordhausen K, Oja H, Taskinen S. Deflation-based separation of uncorrelated stationary time series. *Journal of Multivariate Analysis* 2014;123:214–227.
- [25] Pham DT, Garat P. Blind Separation of Mixture of Independent Sources through a Quasi-maximum Likelihood Approach. *IEEE Transactions on Signal Processing* 1997;45(7):1712–1725.
- [26] Lee S, Shen H, Truong YK, Lewis MM, Huang X. Independent Component Analysis Involving Autocorrelated Sources with an Application to functional Magnetic Resonance Imaging. *Journal of the American Statistical Association* 2011;106:1009–1024.
- [27] Lee S, Shen H, Truong Y. Sampling properties of color Independent Component Analysis. *Journal of Multivariate Analysis* 2020;181:104692.
- [28] Kooperberg C, Stone CJ, Truong YK. Log-spline Estimation of a Possibly Mixed Spectral Distribution. *Journal of Time Series Analysis* 1995;16(4):359–388.
- [29] Dzhaparidze K, Kotz S. *Parameter Estimation and Hypothesis Testing in Spectral Analysis of Stationary Time Series*. Springer; 1986.

- [30] Brillinger DR. *Time Series: Data Analysis and Theory*. Second ed. Society for Industrial and Applied Mathematics; 2001.
- [31] Wahba G. Automatic Smoothing of the Log Periodogram. *Journal of the American Statistical Association* 1980;75(369):122–132.
- [32] Chow YS, Grenander U. A Sieve Method for the Spectral Density. *The Annals of Statistics* 1985;13(3):998–1010.
- [33] Franke J, Härdle W. On Bootstrapping Kernel Spectral Estimates. *The Annals of Statistics* 1992;20(1):121–145.
- [34] Pawitan Y, O'Sullivan F. Nonparametric Spectral Density Estimation Using Penalized Whittle Likelihood. *Journal of the American Statistical Association* 1994;89(426):600–610.
- [35] Fan J, Kreutzberger E. Automatic Local Smoothing for Spectral Density Estimation. *Scandinavian Journal of Statistics* 2001;25(2):359–369.
- [36] Edelman A, Arias TA, Smith ST. The Geometry of Algorithms with Orthogonality Constraints. *SIAM Journal on Matrix Analysis and Applications* 1998;20:303–353.
- [37] Amari SI. Natural Gradient Learning for Over-and Under-complete Bases in ICA. *Neural Computation* 1999;11(8):1875–1883.
- [38] Douglas SC. Self-stabilized Gradient Algorithms for Blind Source Separation with Orthogonality Constraints. *IEEE Transactions on Neural Networks* 2002;11(6):1490–1497.
- [39] Plumbley MD. Lie Group Methods for Optimization with Orthogonality Constraints. *Independent Component Analysis and Blind Signal Separation* 2004;3195:1245–1252.
- [40] Ye M, Fan X, Liu Q. Monotonic Convergence of a Nonnegative ICA Algorithm on Stiefel Manifold. *Lecture Notes in Computer Science* 2006;4232:1098–1106.
- [41] Schwarz G. Estimating the Dimension of a Model. *The Annals of Statistics* 1978;6(2):461–464.
- [42] Amari S, Cichocki A, Yang HH. A New Learning Algorithm For Blind Signal Separation. *Advances in Neural Information Processing Systems* 1996;8:757–763.
- [43] Chang J. *Composing Noise*. Institute of Sonology; 1999.
- [44] Dinno A. Exploring the sensitivity of Horn's parallel analysis to the distributional form of random data. *Multivariate behavioral research* 2009;44(3):362–388.
- [45] Ilmonen P, Paindaveine D. Semiparametrically Efficient Inference Based on Signed Ranks in Symmetric Independent Component Models. *The Annals of Statistics* 2011;39(5):2448–2476.
- [46] Samworth RJ, Yuan M. Independent Component Analysis via Nonparametric Maximum Likelihood Estimation. *The Annals of Statistics* 2012;40(6):2973–3002.
- [47] Kooperberg C, Stone CJ, Truong YK. Rate of Convergence for Log spline Sepctral Density Estimation. *Journal of Time Series Analysis* 1995;16(4):389–401.